Experimental results: The example filter using the proposed CMI was designed and fabricated in an AMI 1.2 μm *n*-well CMOS process. A microphotograph of the chip is shown in Fig. 3. The on-chip capacitors range from 6.5 to 20.8 pF. The single voltage source, V_{gm}, which sets the bias currents of the OTAs is provided externally, so that the unity-gain frequency of CMIs, and hence the cutoff frequency of the filter, can be easily tuned.

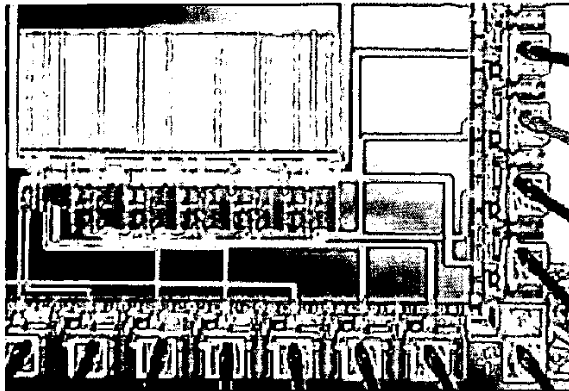

Fig. 3 *Microphotograph of fifth-order Butterworth lowpass filter*

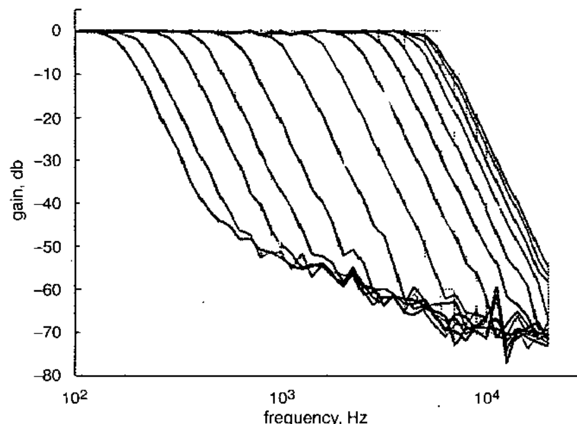

Fig. 4 *Frequency response of fifth-order Butterworth lowpass filter chip for various V_{gm} settings*

The measured frequency response (Fig. 4) shows that the lowpass filter achieves −3 dB cutoff frequencies in the audio frequency range and the cutoff frequency can be varied between 160 Hz and 5.6 kHz using the control voltage V_{gm}. As V_{gm} increases, the curves shift from left to right. Note that cutoff frequency does not increase exponentially as V_{gm} becomes close to or higher than the threshold voltage of bias transistors in OTAs.

The chip was tested using computer-supplied, sinusoidal currents with swept frequencies. In Fig. 4, the noise floor increases with reducing frequency, due to $1/f$ noise in opamps that were used in the test circuitry.

The active filter area is about 0.08 mm^2/pole, including the capacitors. The filter was biased with 100 μA, and the supply voltage was 5 V. The fifth-order filter consumes approximately 20 mW.

Conclusion: A novel current-mode integrator for low frequency continuous-time filters is introduced. It is demonstrated that audio cutoff frequencies could be achieved in a design that well produces the expected characteristics of a fifth-order Butterworth lowpass filter. The cutoff frequencies were shown to be voltage-controllable over a broad frequency range.

Acknowledgments: This work was supported by ONR and DARPA.

© IEE 2003
11 March 2003
Electronics Letters Online No: 20030580
DOI: 10.1049/el:20030580

Z. Yang, T. Hinck, H.I. Cohen and A.E. Hubbard (*VLSI and Neural Networks Systems Laboratory, Department of Electrical and Computer Engineering, Boston University, 8 Saint Mary's Street, Boston, MA 02215, USA*)

E-mail: aeh@bu.edu

References

1 SILVA-MARTINEZ, J., and SALCEDO-SUNER, J.: 'IC voltage-to-current transducers with very small transconductance', *Analog Integr. Circuits Signal Process.*, 1997, **13**, pp. 285–293
2 GARDE, P.: 'Transconductance cancellation for operational amplifiers', *IEEE J. Solid-State Circuits*, 1977, **SC-12**, pp. 310–311
3 SOLIS-BUSTOS, S., SILVA-MARTINEZ, J., MALOBERTI, F., and SANCHEZ-SINENCIO, E.: 'A 60-dB dynamic-range CMOS sixth-order 2.4-Hz low-pass filter for medical applications', *IEEE Trans. Circuits Syst. II*, 2000, **47**, (12), pp. 1391–1398
4 SILVA-MARTINEZ, J., and VAZQUEZ-GONZALEZ, A.: 'Impedance scalers for IC active filters'. Proc. ISCAS'98, Monterey, CA, USA, Vol. 1, pp. 151–154
5 RAMIREZ-ANGULO, J., ROBINSON, M., and SANCHEZ-SINENCIO, E.: 'Current-mode continuous-time filters: two design approaches', *IEEE Trans. Circuits Syst. II*, 1992, Vol. 39, pp. 337–341
6 LEE, S.-S., ZELE, R.H., ALLSTOT, D.J., and LIANG, G.: 'CMOS continuous-time current-mode filters for high-frequency applications', *IEEE J.Solid-State Circuits*, 1993, **28**, (3), pp. 323–328
7 SMITH, S.L., and SANCHEZ-SINENCIO, E.: 'Low voltage integrators for high-frequency CMOS filters using current-mode techniques', *IEEE Trans. Circuits Syst. II*, 1996, **43**, pp. 39–48
8 RAMIREZ-ANGULO, J., and SANCHEZ-SINENCIO, E.: 'High frequency compensated current-mode ladder filters using multiple output OTAs', *IEEE Trans. Circuits Syst. II*, 1994, **41**, (9), pp. 581–586
9 TOUMAZOU, C., LIDGEY, J., and HAIGH, D.: 'Analogue IC design – The current-mode approach' (IEE, London, April 1990)

Monolithic micropower amplifier using SiGe *n*-MODFET device

A. Vilches, K. Fobelets, K. Michelakis, S. Despotopoulos, C. Papavassiliou, T. Hackbarth and U. König

A micropower-relevant model is extracted from the DC characteristics of an *n*-type buried channel Si/SiGe hetero-junction modulation doped FET (HMODFET). This model is then used to design a novel monolithic SiGe single-stage class-A power amplifier for micropower operation (sub 500 μW). The amplifier is fabricated and measured data of the power-gain against operating power are presented for the first time.

Introduction: Research on SiGe HMODFETs is motivated by their compatibility with existing CMOS fabrication technology and the promise of superior high-frequency transistor performance when compared to conventional MOSFETs [1]. SiGe HMODFETs contain a buried channel in high mobility strained Si, separated from the gate by further semiconductor layers [2]. The strain in the buried channel and the removal of the carriers from the SiO_2 interface result, in that for a given gate bias, the transconductance (g_m) increases more rapidly than is the case for Si MOSFETs and is always higher than in conventional FETs [3]. The extra boost in g_m at low bias levels warrants the use of these devices in micropower applications where battery life is of prime importance [4]. In this Letter we report on a fabricated, SiGe single-stage class-A amplifier, for operation at micropower levels, consisting of a monolithically integrated 0.5 × 100 μm *n*-MODFET and resistive 100 Ω load.

Device structure and characteristics: The *n*-MODFET structure (see Table 1) was grown by molecular beam epitaxy (MBE) on a 40%

Ge-graded virtual substrate (VS), which was prepared by low energy plasma enhanced chemical vapour deposition (LEPECVD).

Table 1: MODFET device structure

3.5 nm Si cap
6 nm SiGe cap 40%
5 nm n^+-SiGe 40%:Sb supply
3.5 nm SiGe 40% spacer
9 nm Si channel
4 nm SiGe 40% spacer
5 nm n-SiGe 40%:Sb supply
150 nm SiGe 40%
LEPECVD 40% 5 μm
Silicon substrate: *p*- > 1000 Ωcm
Total MBE Epi: 186 nm

A standard fabrication technique for *n*-type SiGe MODFETs was applied, which included dry mesa etching for electrical isolation of the epitaxial active areas and deposited field oxide for electrical isolation of the implanted areas. The ohmic contacts' implant was P activated by low temperature rapid thermal annealing (RTA). The ohmic contacts consist of Ti/Pt/Au and this metal also serves for the circuit interconnections. The Schottky gates were defined by e-beam lithography and liftoff and consisted of Pt/Au. The minimum gate length available on-wafer was 0.1 μm and a number of test devices and structures were available for characterisation including Hall patterns, which were all measured at 300 K. The sheet resistivity of the structure was 811 Ω/sq, the sheet electron density was $4.5 \times 10^{12}\,cm^{-2}$ and the corresponding mobility was $1700\,cm^2/V$ (300 K).

Device modelling: Measured DC current–voltage data was entered into MWOFFICE (Electronic CAD package) [5] and the software was used to successfully fit a Curtice [6] type equivalent circuit model (Fig. 1), for operation on micropower supply in the V_{DS} range of 0 to 0.5 V and V_{GS} range of −0.5 to 0 V, having established that the device threshold voltage is −0.5 V.

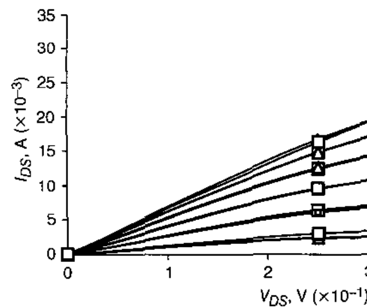

Fig. 1 *Measured against modelled device output characteristics for $V_{GS}=-0.5$ to 0 V*
□ measured
△ modelled

Amplifier design: The single-stage amplifier was simulated in MWOFFICE using the extracted micropower model with an input power level of −40 dBm. The FET is worked into a resistive 100 Ω load and no microwave matching components were used in the initial design as the circuit's bandwidth was expected to be low at the power operation levels targeted. The circuit's input and output are terminated with standard 50 Ω ports and the simulation showed that a maximum transducer power gain of 30 dB, G_{MAX} (see (1)), was achievable with a bias of $V_{GS}=-0.2$ V and $V_{DS}=0.3$ V (sub 500 μW total power supplied):

$$G_{MAX} = \frac{|S_{21}|}{|S_{12}|}(k - \sqrt{k^2-1}) \quad (1)$$

where

$$k = \frac{1 - |S_{11}|^2 - |S_{22}|^2 + \Delta^2}{2|S_{12}||S_{21}|} \quad (2)$$

and

$$\Delta = S_{11}S_{22} - S_{12}S_{21} \quad (3)$$

Amplifier characterisation: A HP5783D network analyser was used to probe, bias and measure the fabricated monolithic amplifier, a picture of which is shown in Fig. 2. Two-port *s*-parameters were recorded and converted, using MWOFFICE, into G_{MAX} against frequency graphs for each power supply level investigated and a chart of measured power gain at the half-power bandwidth frequency against power supplied is shown in Fig. 3. The graph illustrates that for a supplied power of only 26 μW, a power gain of ~15 dB is available with an operating bandwidth of 38 MHz.

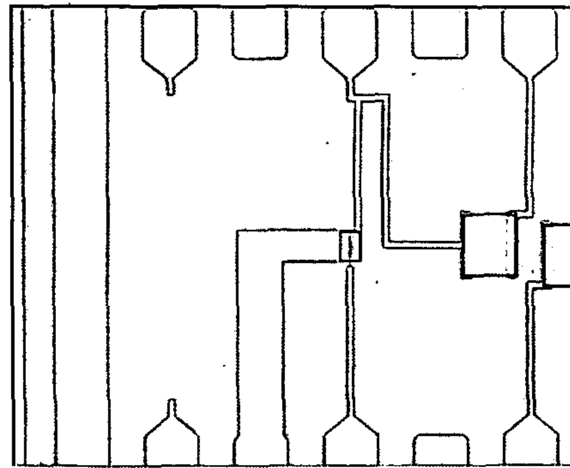

Fig. 2 *Micrograph of fabricated SiGe amplifier on-wafer*

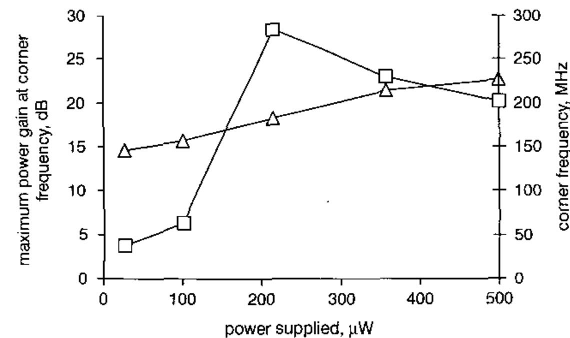

Fig. 3 *Measured amplifier response for micropower operation*
–△– maximum power gain at corner frequency
–□– corner frequency

Conclusion: A SiGe *n*-MODFET device has been fabricated, measured and a micropower-relevant model extracted for use in the design of a monolithic single-stage class-A amplifier. The SiGe amplifier was fabricated and a graph of measured maximum power gain against power supplied has been presented for the first time. A minimum operating power of 26 μW resulted in a measured power gain of ~15 dB with a corner frequency of 38 MHz.

Acknowledgment: Financial support from EPSRC award GR/N65844/01 is gratefully acknowledged.

© IEE 2003
10 April 2003
Electronics Letters Online No: 20030581
DOI: 10.1049/el:20030581

A. Vilches and K. Fobelets (*Optical and Semiconductor Devices, Department of Electrical and Electronic Engineering, Imperial College London, Exhibition Road, London SW7 2BT, United Kingdom*)

E-mail: a.vilches@imperial.ac.uk

K. Michelakis, S. Despotopoulos and C. Papavassiliou (*Analogue Electronics, Department of Electrical and Electronic Engineering, Imperial College London, Exhibition Road, London SW7 2BT, United Kingdom*)

T. Hackbarth and U. König (*Daimler Chrysler Research Center, D-89081 Ulm, Germany*)

References

1 O'NEILL, A.G., and ANTONIADIS, D.A.: 'Investigation of Si/SiGe-based FET geometries for high frequency performance by computer simulation', *IEEE Trans. Electron Devices*, 1997, **44**, pp. 80–88

2 GLUCK, M., HACKBARTH, T., KÖNIG, U., HAAS, A., HOCK, G., and KOHN, E.: 'High fmax *n*-type Si/SiGe MODFETs', *Electron. Lett.*, 1997, **33**, (4), pp. 335–337

3 PAPAVASSILIOU, C., FOBELETS, K., and TOUMAZOU, C.: 'SiGe hetero-FET potential for micro-power applications', *invited paper, IEICE Trans. Electron.*, (E00-A(2000))

4 LENK, J.D.: 'Simplifier design of micropower and battery circuits' (Butterworth-Heinemann, December 1995) ISBN 0750695102

5 http://www.mwoffice.com/

6 CURTICE, W.R.: 'A nonlinear GaAs FET model for use in the design of output circuits for power amplifiers', *IEEE Trans. Microw. Theory Tech.*, 1983, **33**, p. 1383

Accurate low-cost measurement technique for occupational exposure assessment of base station antennas

W. Joseph, L. Verloock and L. Martens

A new technique for near field measurements around wireless base station antennas is presented. Using these safety measurements the compliance boundaries of a base station are determined and compared with FDTD simulations. Excellent agreement is reported. The measurements are performed in a non-anechoic measurement site which results in a low-cost method.

Introduction: To determine the safety compliance boundaries for occupational exposure of a base station antenna, the electromagnetic fields around the base station antenna must be determined and be compared to the reference levels [1]. Therefore it is important to be able to perform accurate electromagnetic field measurements close to the source. Both electric and magnetic field have to be determined when performing measurements in the near field of the base station [1, 2]. Mostly, antenna radiation measurements are performed in an anechoic chamber. However, this is expensive. The measurements described in this Letter are planar near-field measurements performed in an indoor open-site surrounded by absorbers to minimise interference. To obtain accurate results, residual reflections due to the non-anechoic property of the measurement site are eliminated with a de-embedding method. This makes it a low-cost method delivering accurate results.

Configuration: We investigate a Kathrein 736863 GSM base station antenna in free space at 947.5 MHz. At this frequency the antenna radiates maximally. We determine the compliance boundaries in front of the antenna because they will be most restrictive for this case. This compliance boundary, noted as D_{front}, defines the boundary outside which the exposure levels of the field do not exceed the reference value in front of the antenna. The measurements are performed with a network analyser (Rohde & Schwarz ZVR). Thus, we consider the combination of base station antenna and measurement probe as a two-port network (see Fig. 1*a*). Fig. 1*b* shows the antenna and the coordinate system used. We use a robot with an accuracy of 0.025 mm to position the probe. The measurements are performed with a spatial grid of 2 cm, smaller than $\lambda/10 = 3.2$ cm at 947.5 MHz. By rotation of the measurement probe three orthogonal components of the field at each position are measured. A selection of measurement probes with a disturbance required to be lower than 5% for near-field exposure measurements around the base station is made [3]. For electric-field measurements a 2.2 cm dipole with a thickness of 0.5 mm has been selected. For the magnetic-field measurements a split-shield loop antenna with diameter of 1.3 cm and thickness of 0.5 mm has been designed. The split-shield loop antenna is chosen to reject the contribution of the electric field to the magnetic-field measurement [4]. The measurement probes are calibrated using a three-antenna method. The antenna factor (AF) of the 2.2 cm dipole and the 1.3 cm loop probe is respectively 64.52 dB(1/m) and 63.88 dB(1/m). These values are relatively high (lower sensitivity) due to the small dimensions of the measurement probes. These small dimensions are necessary for a satisfying spatial resolution and for a disturbance that is lower than 5%.

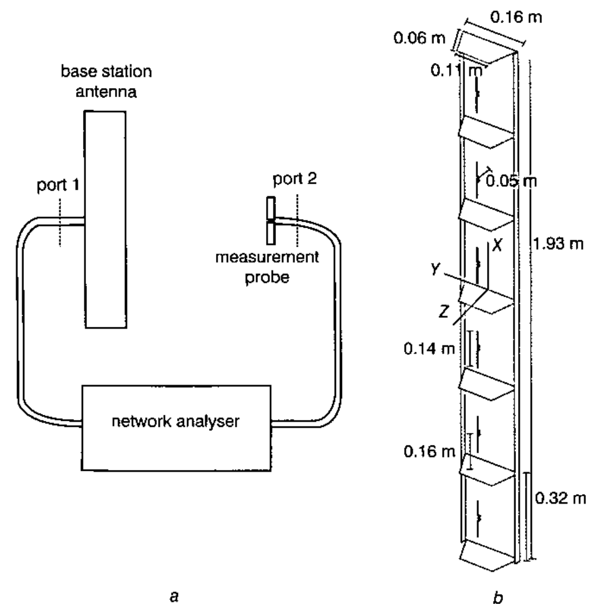

Fig. 1 *Combination base station antenna and measurement probe as two-port network and dimensions of K736863 antenna*

a Combination base station antenna and measurement probe
b Dimensions of K736863 antenna

Theory of method: When the S_{21}-parameters are measured for three orthogonal components, the total field at a certain measurement point can be expressed as the following:

$$|X^{meas}_{tot}| = \sqrt{50 \cdot P_i} \cdot 10^{\mathrm{AF}_X/20} \cdot \sqrt{|S_{21}|_1^2 + |S_{21}|_2^2 + |S_{21}|_3^2} \quad (1)$$

with

X is the E or H, the magnitude of the electric or magnetic field, P_i is the available input power, AF_X is the antenna factor of the dipole or the loop probe, and $|S_{21}|_i$ is the magnitude of S_{21} related to the orthogonal component i ($i = 1, 2, 3$).

Because of the non-anechoic property of the measurement site we have to take into account residual reflections. To this end we perform a de-embedding step. For each orthogonal component of the field at each measurement position we perform a measurement from 300 kHz up to 4 GHz. We use this large frequency range of $\Delta f = 3.9997$ GHz to obtain enough resolution in the time domain to distinguish the direct and reflected beams. Using a tenth-order Butterworth band-pass filter the $S_{21}(f)$-parameters in the desired frequency range are obtained. We then take the inverse FFT transform to derive $s_{21}(t)$. Next, we apply a time-domain gating technique [5] to eliminate the residual reflection. The reflections in $s_{21}(t)$ are suppressed by a tenth-order Butterworth digital band-pass filter. This type of filter is selected because of its flat pass-